Chemical mixing at "Al on Fe" and "Fe on Al" interfaces

P. Süle, D. Kaptás, L. Bujdosó, Z. E. Horváth, A. Nakanishi, and J. Balogh

Articles you may be interested in

Chemical mixing at "Al on Fe" and "Fe on Al" interfaces

P. Süle,[1] D. Kaptás,[2] L. Bujdosó,[2] Z. E. Horváth,[1] A. Nakanishi,[3] and J. Balogh[2]

[1]*Institute of Technical Physics and Materials Science, Centre for Energy Research,*
Hungarian Academy of Sciences, H-1525 Budapest, P.O. Box 49, Hungary
[2]*Institute for Solid State Physics and Optics, Wigner Research Centre for Physics,*
Hungarian Academy of Sciences, H-1525 Budapest, P.O. Box 49, Hungary
[3]*Department of Physics, Shiga University of Medical Science, Shiga 520-2192, Japan*

The chemical mixing at the "Al on Fe" and "Fe on Al" interfaces was studied by molecular dynamics simulations of the layer growth and by ^{57}Fe Mössbauer spectroscopy. The concentration distribution along the layer growth direction was calculated for different crystallographic orientations, and atomically sharp "Al on Fe" interfaces were found when Al grows over (001) and (110) oriented Fe layers. The Al/Fe(111) interface is also narrow as compared to the intermixing found at the "Fe on Al" interfaces for any orientation. Conversion electron Mössbauer measurements of trilayers—Al/^{57}Fe/Al and Al/^{57}Fe/Ag grown simultaneously over Si(111) substrate by vacuum evaporation—support the results of the molecular dynamics calculations. © 2015 AIP Publishing LLC. [http://dx.doi.org/10.1063/1.4932521]

I. INTRODUCTION

Interfaces play a decisive role in all the physical properties of nanometer scale layer structures, and with the increase of computers' speed, the *ab initio* calculation and the atomistic simulation of the interface formation during the atomic deposition process became a feasible theoretical approach.[1] The common tools are the atomic potential calculation based on quantum mechanics theory and the atomistic simulation by molecular dynamics (MD) algorithm. Within reasonable computation time, the calculations can be made over an area of just a few square nanometers, and it usually starts with a perfect substrate layer. The experimental methods most frequently used to characterize the multilayer interfaces, e.g., grazing incidence X-ray reflectivity (XRR), Rutherford backscattering (RBS), or Auger electron spectroscopy, etc., sample much larger area and cannot make clear distinction between the topological roughness and/or waviness of the layers and the chemical mixing of them. This way a quantitative comparison of the experimental and the MD results is not unambiguous. Mössbauer spectroscopy (MS) and other nuclear methods, which are sensitive to the atomic scale neighborhood of a specific isotope, can give unique information on the extent of the chemical mixing and on the nature of the compound phases formed at the interface without being significantly disturbed by topological features of the layers.

The aim of this work is to perform MD simulation of the Fe interface formation in a system where significantly different chemical mixing is expected at the top and the bottom interface of the Fe layer and to compare the concentration distribution calculated along the growth direction with that inferred from MS measurements. The Fe-Al system is selected for this purpose since the largely different chemical mixing at the top and the bottom interface has been established by different experimental methods.[2–4] The interface mixing in Fe-Al multilayers has been studied intensively by MS,[5–10] as well, and due to the outstanding properties of the

alloy system for industrial applications, the Mössbauer parameters of the different alloy phases and the dependence of the hyperfine fields (HFs) on the number of Al neighbors in the *bcc* phase are well studied.[8] MD simulations have already been performed for the Fe(001)/Al (Al on top of Fe) and Al(001)/Fe (Fe on top of Al) interfaces,[11,12] and these indeed show an asymmetry of the top and bottom Fe interfaces. It can be explained by the largely different energy barriers of the surface diffusion and the incorporation process for the two different cases.[13] Now, we performed MD simulations for all possible crystal orientations.

In Mössbauer spectroscopy, the top and the bottom interface of a Fe layer has generally been distinguished by the ^{57}Fe marker method,[5,14,15] in which case the position of a thin ^{57}Fe layer (the Mössbauer isotope) is varied across the natural Fe layer. The application of this method is limited by the possible mixing and diffusion between the ^{57}Fe marker and the natural Fe layers, and in case of an extended interface, the quantitative conclusion is difficult. The use of an auxiliary layer prepared from an element non-mixing with iron, e.g., Ag, and the comparison of M/^{57}Fe/M and M/^{57}Fe/Ag samples—where M can be any kind of material—was suggested recently[16] as a strategy to gain quantitative results on the difference between the top and the bottom Fe interface. The idea is very simple; if the top and the bottom interfaces are similar in an M/Fe/M trilayer, then the hyperfine parameters of the respective spectral component remain unaltered and the intensity of the interface sub-spectrum is halved when the top M layer is replaced by Ag. Deviation from this expectation indicates that the distribution of the elements is different across the top and the bottom interface, which is often termed shortly as interface asymmetry. The non-mixing Ag layer modifies the hyperfine parameters of only 2–3 Fe monolayers (MLs),[17] which can be taken into account. One should remark that some mixing of Ag and Fe can take place during the non-equilibrium processes of thin film growth,[18] but these processes cause a very limited

mixing mainly at the "Fe on Ag" interface[19] due to the smaller surface energy of Ag than that of Fe and do not affect our results.

II. CALCULATION METHODS

Classical molecular dynamics has been used as implemented in the LAMMPS code (Large-scale Atomic/Molecular Massively Parallel Simulator).[20] Isobaric-isothermal (NPT ensemble) simulations (with Nose-Hoover thermostat and a prestostat) were carried out at 300 K. Vacuum regions were inserted above and below the slab of the substrate system to ensure the periodic conditions not only in lateral directions (x, y) but also in the direction perpendicular to the substrate's surface (z). The temperature of the substrate has been kept at 300 K. The variable time step algorithm has been exploited. The code OVITO[21] has been utilized for displaying atomic and nanoscale structures. The flux of the deposited atoms was maintained as 2.25×10^{25} atoms/s/cm^2 (one particle per 10 k simulation steps). In total, at least 10–15 MLs of adatoms were deposited on the substrate in which each ML corresponded to nearly 100 adatoms for the Fe/Al and Al/Fe systems. The substrate's surface was 3×3 nm^2. For Fe and Al, the embedded-atom method (EAM) potentials have been used as generated by the EAM database tool[22] provided by the code LAMMPS. For the FeAl cross-interaction, the mixing rule of Johnson[23] has been utilized, which provides reasonable alloy properties. The EAM potential has been tested for fcc and bcc elemental and cubic alloy phases. Reasonable properties have been found for lattice constants, cohesive properties, and melting temperature. For the B2 alloy phase of FeAl 0.28 eV/atom, cohesive energy is calculated, which is comparable with the *ab initio* DFT calculated 0.26–0.33 eV/atom.[24] The lattice constant is also nicely reproduced (2.90 Å vs. the 2.87 Å DFT and 2.91 Å experimental value).[24]

The simulated growth of the film has been carried out using gentle conditions. In every 10 k (few ps) simulation steps, a new vapor atom has been added to the vacuum region well above the substrate. For each inserted particles, downward velocities are given, which correspond roughly to 0.1 eV kinetic energy. Therefore, the incoming film atoms have been evaporated and slowly condensed to the substrate's surface. The evaporation takes place 6–8 nm above the growing film. The applied mild conditions of the deposition allow the slow growth of the film without artificial effects such as particle insertion in the growing film. Therefore, we can rule out artificial intermixing (IM) due to harsh conditions during simulated film growth. The few bottom layers of the substrate have been fixed in order to avoid the rotation and/or the translation of the system. The simulated film growth has been applied for (111), (110), and (001) orientations of the substrate surfaces. Our purpose was to monitor the dependence of IM upon the crystallographic orientation of the surface.

III. EXPERIMENTAL METHODS

The experimental investigations were performed on tri-layer samples prepared by vacuum evaporation of the elements over a Si(111) substrate. The parameters of the evaporation chamber are detailed in Ref. 8. The deposition rates were about 0.1 nm/s. The two sample pairs studied have the following layer sequences:

1A. Si(111)/20 nm Al/3.5 nm ^{57}Fe/20 nm Al
1B. Si(111)/20 nm Al/3.5 nm ^{57}Fe/10 nm Ag/10 nm Al
2A. Si(111)/20 nm Al/5.0 nm ^{57}Fe/20 nm Al
2B. Si(111)/20 nm Al/5.0 nm ^{57}Fe/10 nm Ag/10 nm Al.

The ^{57}Fe layers of samples A and B were prepared simultaneously to ensure the equal width of the ^{57}Fe layers of the sample pairs. The W crucible used for the evaporation of ^{57}Fe enriched iron was in equal distance to the two substrates. The respective Al layers of the sample pairs were also prepared simultaneously, but the asymmetric positions of the two electron guns relative to the substrate holders can result in some difference (less than 1 nm) of the Al layer thicknesses. The Al layers on top of the Ag layers in case of the 1B and 2B samples were deposited in order to increase the stability of the ^{57}Fe layers against oxidation.

Structural analysis was performed on sample 2A by X-ray diffractometry (XRD) of Cu K$_\alpha$ radiation in a Bruker AXS D8 Discover diffractometer equipped with Göbel-mirror and a 2D position sensitive (GADDS) detector system.[25] The intensity was acquired at two detector positions at nominal 2θ angles of 40° and 60°, covering the range of about 28°–72°, while the sample was positioned at $\theta = 20°$ and 30°, respectively.

The conversion electron Mössbauer spectroscopy (CEMS) measurements were carried out by using a conventional constant acceleration-type spectrometer. The spectra were measured by a 50 mCi ^{57}Co(Rh) single line source, and a 96%He-4%CH$_4$ gas mixture was used for the detection of the conversion electrons at room temperature. The HF distributions were evaluated according to the Hesse-Rübartsch method,[26] i.e., fitting the amplitudes of a number of sextets with HFs increasing with an equal step value. The isomer shift (IS) values are given relative to that of α-Fe at room temperature.

IV. RESULTS

In Figs. 1 and 2, the simulation cells are shown after classical MD simulations for various orientations of the
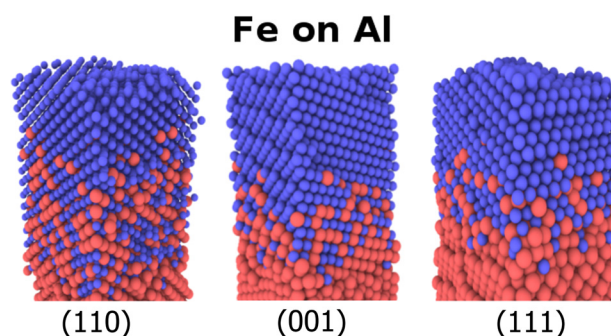

Fe on Al

(110)   (001)   (111)

FIG. 1. Typical broadened interfaces obtained by MD simulations of the Fe layer growth on Al for different substrate orientations. Dark (blue) and light (red) spheres are the Fe and Al atoms, respectively.
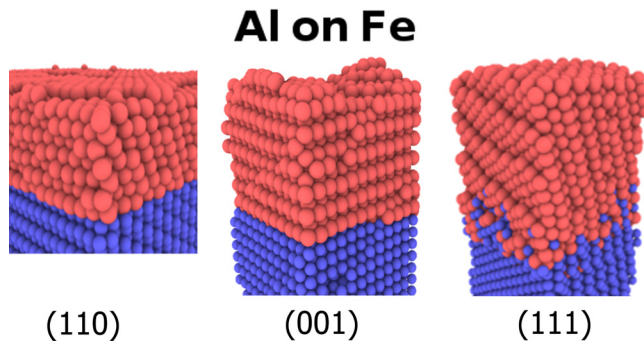
FIG. 2. Typical interfaces obtained by MD simulations of the Al layer growth on Fe for different substrate orientations. Dark (blue) and light (red) spheres are the Fe and Al atoms, respectively.

FIG. 4. The Al depth profiles obtained from the MD simulations for various Fe substrate orientations.

substrates, while Figs. 3 and 4 show the calculated depth profiles of Fe and Al, respectively. When energetic Fe atoms with 0.1 eV kinetic energy were evaporated on the *fcc* Al surface, a strong IM has been found along the growth direction, as it can be seen in Figs. 1 and 3. The IM is especially large on the Al(110) surface. In this case, the width of the interface is around 3 nm, while for the other two orientations, it is slightly less than 2 nm. Allowing further energetic Fe atom impacts, the width of the interface increases for the (110) orientation, while it remains nearly unchanged for the (001) and (111) orientations. The significant orientation dependency of the IM can be due to the fact that the (001) and (111) surfaces are more closely packed than the (110) one for *fcc* crystals. The (110) orientation might promote the opening of channels for atomic migration, and therefore the steady state has not been reached with the available computer capacity.

In the reverse case, when Al atoms were deposited on the surface of *bcc* Fe, the interface is very sharp (see Figs. 2 and 4) for (001) and (110) Fe orientations, and slightly broader, about 0.5 nm for (111) orientation. Therefore, a very strong asymmetry can be seen between the IM at the "Fe on Al" and the "Al on Fe" interfaces.

Fig. 5 shows the acquired XRD intensities of sample 2A, as well as the positions of the *bcc* Fe and *fcc* Al peaks

falling in the 2θ range of the measurement. Two peaks are visible, at about $\theta = 38.5°$ and $\theta = 44.5°$, and they can be identified as Al(111) and Fe(110), respectively. The lack of other peaks indicates that both the Al and the Fe layers are textured. The inset of Fig. 5 shows the frame of the 2D detector with the two arcs corresponding to the reflections found. Sections of the Debye rings corresponding to reflections with increasing scattering angle appear from right to left. If random crystallite orientation is present, uniform intensity distribution along the diffraction arc is expected. Intensity maximum around the middle part of the arc, like in our case, indicates a fiber texture with diffracting lattice plane preferentially parallel to the substrate. The (111) texture is quite often formed over various substrates, and in case of pure silicon substrate, the epitaxial growth of Al with Al(111)//Si(111), Al[$\bar{1}$10]//Si[$\bar{1}$10] epitaxial relation[27] is also feasible. The Fe(110) reflection is weak and wide owing to the small layer thickness.

The CEMS spectra of the four samples measured at room temperature are shown in Fig. 6(a) and the evaluated normalized HF distributions in Fig. 6(b). The spectra were
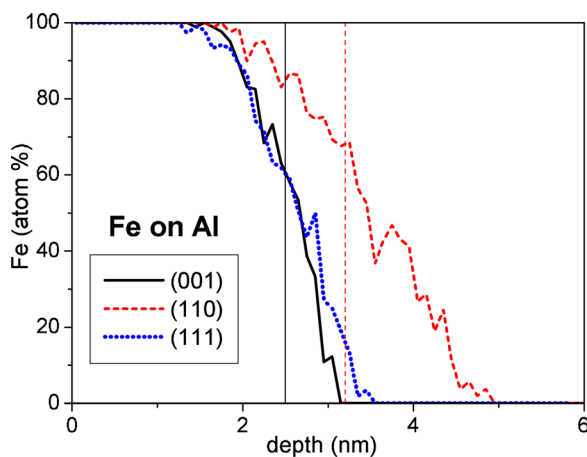

FIG. 3. The Fe depth profiles obtained from the MD simulations for various Al substrate orientations. The original positions of the Al surface are also shown for the (001) and (111) orientations with continuous thin (black) line and with a thin dashed (red) line for the (110) orientation.
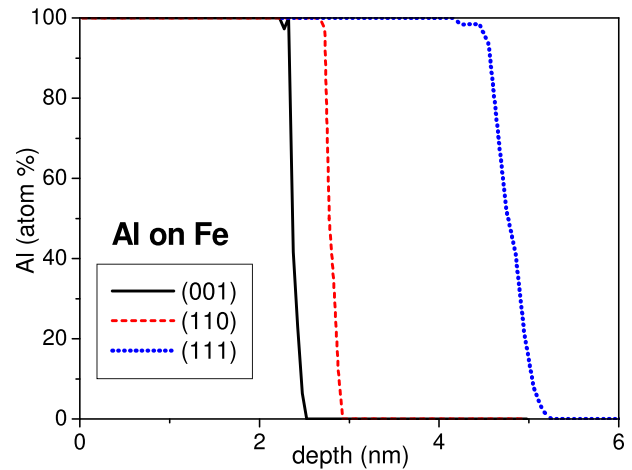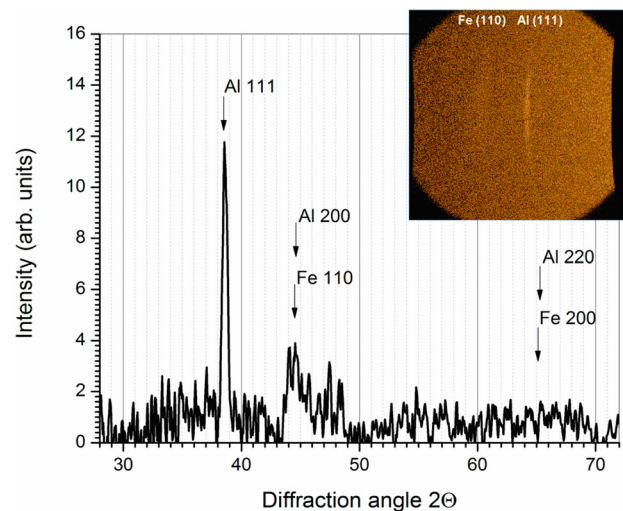

FIG. 5. XRD pattern of sample 2A. The inset shows the frame of the 2D detector with the two arcs corresponding to the reflections found.
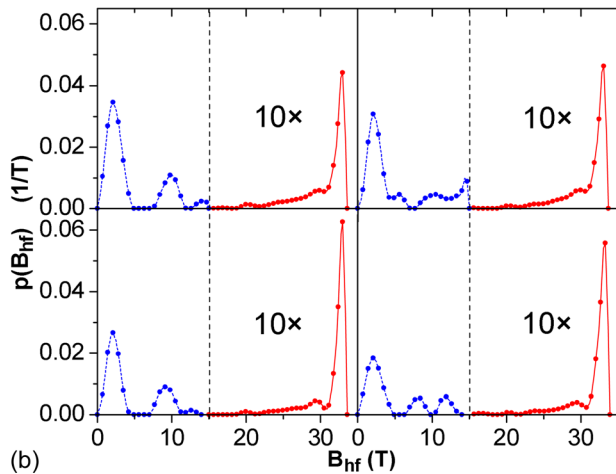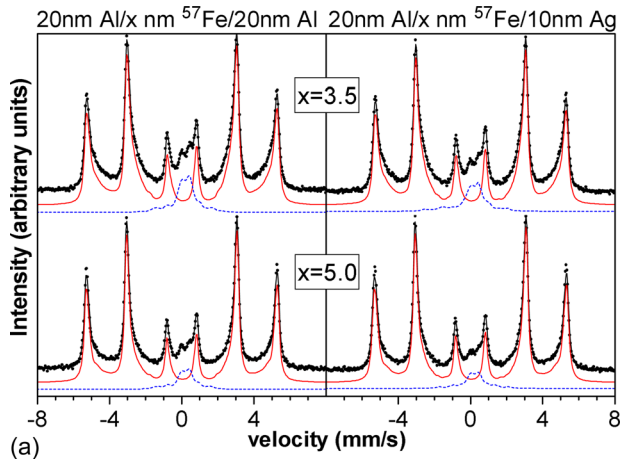
(a)

(b)

FIG. 6. Mössbauer spectra measured at room temperature (a) and the calculated HF distributions (b). Dashed (blue) lines show the subspectra/HF distributions for the nonmagnetic Fe atoms and the continuous (red) lines for the magnetic Fe atoms (see text for an explanation). Note that the distributions are shown on y-scales 10 times magnified above 15 T (indicated by the dashed lines).

best described by two separate HF distributions allowing magnetic sextets below and above 15 T; the respective spectral components are shown in Fig. 6(a). The spectral areas of the components belonging to the distributions below and above 15 T are roughly proportional to the number of non-magnetic and magnetic Fe atoms,[8] respectively. In the evaluations, all the line-width was fixed to 0.24 mm/s, and the step value was fixed to 0.7 T for the low field distribution and was allowed to vary for the high field part; it was around 0.62 T for all the spectra. The isomer shifts were supposed to be proportional to the HFs, the lower the HF the higher the isomer shift is for both distributions. The intensities of the second and fifth lines of the sextets are close to 4 for each case.

The HF distributions are shown in Fig. 7 for all the four spectra of Fig. 6 after the probabilities have been multiplied by the Fe layer thickness of the specific sample. This way, the normalized spectral intensities of the HF components are transformed into layer thickness ratios of the HF components, and the sum over the distribution gives the total amount of Fe measured in layer thickness equivalent. Concerning the question of interface asymmetry, the most
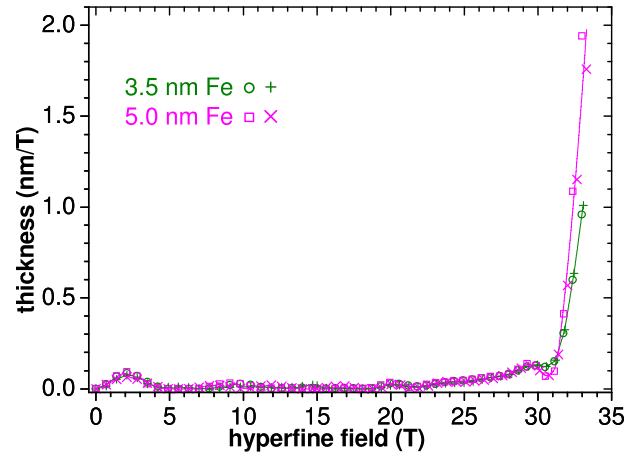

FIG. 7. Hyperfine field distributions of Fig. 6 multiplied by the nominal Fe layer thickness of the samples. The circles, squares, plus signs, and × marks show the data for samples 1A, 2A, 1B, and 2B, respectively.

remarkable feature of Fig. 7 is the overlap of the distributions in the whole HF range for the equal Fe thickness sample pairs. This observation means that in regard of the short range order, the "Al on Fe" interface of samples 1A and 2A is as sharp as the "Ag on Fe" interfaces of samples 1B and 2B, i.e., chemical mixing takes place only at the "Fe on Al" interface.

Below 30 T field, the distributions undoubtedly characterize a chemically intermixed region of the Fe layers, and there is a remarkable overlap of the HF distributions of Fig. 7 in this range for all the four samples. The agreement of the distributions below 30 T field for samples 1A and 2A shows that the formation of the intermixed region is completed for Fe layer thickness equal or less than 3.5 nm, i.e., it contains equal or less Fe than a 3.5 nm thick Fe layer. The broad HF distribution of the intermixed region indicates a wide Al concentration distribution. The small peak around 2.1 T field does not in fact originate from a magnetic splitting but simulates a quadrupole doublet with a splitting around 0.47 mm/s and IS 0.22 mm/s, parameters that are similar to those observed for the single component appearing in case of ultrathin (0.3–0.4 nm) Fe layers.[8] The amount of Fe represented by this peak is in between 0.2 nm and 0.3 nm, as measured in Fe layer thickness equivalent, for all the four samples. The components around 10 T field are due to those nonmagnetic Fe atoms that have magnetic Fe neighbors[8] and experience a HF due to the conduction electron polarization. These Fe atoms make a small (0.1 nm) but well reproduced fraction in all four spectra. The magnetic Fe atoms are represented by HF components above 15 T field. The HF of the magnetic Fe atoms largely depends on the magnetic moments of the first and second neighbor Fe atoms as well,[8] i.e., the local distribution of the Al atoms in the intermixed region, which explains the broad distribution in the 20–30 T field range. The Al concentration of the magnetic region is not easy to estimate from the Hfs since the concentration is certainly non-homogeneous along the growth direction and this way the distribution is far from a simple binomial one.

The largest spectral intensities are observed above 30 T field for all the samples, and it is only this part of the

distribution that varies on increasing the Fe layer thickness. The 33 T field component can be attributed to Fe atoms that have no Al or Ag neighbors in the first two coordination shells. Such Fe atoms should appear after the formation of two monolayers of Fe. The intensity of this sextet is 27% and 29% for samples 1A and 1B and 39% and 35% for samples 2A and 2B, i.e., about 1.0 and 1.8 nm in equivalent layer thickness, for the 1 and 2 type samples, respectively. One Al neighbor in the first coordination shell reduces the HF of a Fe atom by 2.3 T and Al neighbors in the second and farther coordination shells can modify this value up to 3 T in the *bcc* alloy phase.[28] These figures are very close for different non-magnetic impurities in *bcc*-Fe,[29] but at interfaces, all the above HF values can be slightly modified by dipolar fields[30] or atomic volume changes due to defect sites. Nevertheless, if we estimate the amount of Fe atoms without Al or Ag first neighbors from the intensity of the components above 30.7 T, it is 58% and 61% for samples 1A and 1B and 71% and 75% for samples 2A and 2B, i.e., the thickness of the pure *bcc*-Fe layer is 2.0, 2.1, 3.5, and 3.7 nm for the four samples, respectively. This analysis is supported by the good agreement of the calculated increase of the pure *bcc*-Fe layer with the nominal increase of the deposited Fe thickness, 1.5 nm from sample 1 to sample 2, and provides about 1.5 nm for the thickness of the intermixed Fe layer. Taking into account an about 0.4 nm perturbed layer at the Ag interface, the thickness of the intermixed Fe region is 1.1 nm at the "Fe on Al" interface. If we suppose a $Fe_{50}Al_{50}$ average concentration of the interface, it makes around 2.7 nm full width.

V. DISCUSSION

The concentration depth profile calculated from our MD simulation agrees well with that of Chung and Chung[11] for Al(001), and the larger intermixing in case of Al(110), as well as the atomically sharp interface over Fe(001) substrates, is also reproduced. Our calculations, although not shown here, also support that increasing the incident energies from 0.1 eV up to 3 eV does not change the concentration depth profiles. In addition to these results, our calculations show that the largely different mixing at the "Fe on Al" and the "Al on Fe" interfaces holds for all possible crystal orientations, i.e., for polycrystalline samples, as well.

The results of the Mössbauer measurements are in agreement with the main features of the concentration distributions calculated from the MD simulations as shown in Figs. 2 and 4. The Mössbauer analysis undoubtedly shows that the "Al on Fe" interfaces of our samples are very sharp on the atomic scale. Since the XRD signal coming from the Fe layer is very weak, it is not yet certain if this holds for all possible crystal orientations or only for the most probable Fe(110) orientation over the (111) textured Al bottom layer. Also, further experiments are necessary to explore if the slight orientation dependence indicated by the MD simulations for the "Al on Fe" interface can be justified. In any case, our results demonstrate that the chemical affinity of the elements plays a negligible role in the interface formation, and the "Al on Fe" interface is just as sharp as the "Ag on

Fe" interface. In case of the "Fe on Al" interface, the about 2.7 nm full width deduced from the Mössbauer results is slightly larger than the around 2 nm calculated width of the intermixed region on Al(111) (see Fig. 2). The contribution of some Al(110) grains due to the non-perfectly textured Al layer, grain boundary regions, or a higher than 50 at. % average Fe concentration of the interface can equally explain it.

The observed chemical sharpness of the "Al on Fe" interface—deduced from our measured Mössbauer spectra and calculated both from our and some previous[11,12] MD simulations—is more pronounced than those reported earlier with the application of different measuring and sample deposition techniques,[2,4,5] including Mössbauer spectroscopy, as well. The comprehensive work of Buchanan *et al.*[2] found 0.9 nm intermixing length for the "Al on Fe" interface. From the latest RBS and XRR results,[4] 2.06 nm width of the "Al on Fe" interface is deduced, contrary to the atomically sharp interface we observe. Most of the former Mössbauer experiments[6–10] studied multilayered samples and therefore were not suitable to make a clear distinction between the two types of interfaces. Jani *et al.*[9] interpreted their Mössbauer results supposing the formation of extended interfaces, but with different concentrations of the two types of interfaces: the "Fe on Al" being Fe-rich and magnetic, while the "Al on Fe" being Al-rich and non-magnetic. Our results definitely exclude such an interpretation. The Mössbauer study of Geilman *et al.*[5] applying the ^{57}Fe marker layer method for single Fe layers has found an extended (around 1.5 nm in equivalent Fe thickness) intermixed region at the "Al on Fe" interface in case of pulsed laser deposited samples over Si(111) substrate with thick (200 nm) Si_3N_4 buffer layer. It should be further studied to what extent the contradictory results are explained by the different sample deposition and interface characterization techniques.

The observed large interface asymmetry can originate from the difference of several physical parameters; mostly, the role of the energy barriers for surface diffusion and incorporation processes, and the local acceleration mechanism has been emphasized.[11–13] Recent MD studies suggested the role of the atomic size and mass difference in the asymmetric behavior of some other bilayer systems on the course of energetic bombardments.[31–33] This mechanism seems less relevant during interface growth, but due to the local acceleration process,[11] certain elements of what is outlined for energetic atoms can also be applicable with some modifications. The different crystal structure of Fe and Al might also contribute to the interface asymmetry developed during the layer growth. The *fcc* surfaces are more closely packed than the *bcc* ones and thus exhibit more ductility and deform more readily under non-equilibrium conditions. This is because the lattice structures with closely packed planes allow more plastic deformation than those that are not closely packed,[34] and it is also easier for atomic planes to slide by each other. These properties facilitate the atomic exchange process during layer growth, since it induces various deformations and atomic rearrangements. The more accurate and detailed understanding of these processes, however, goes beyond the scope of the present paper.

VI. CONCLUSION

Molecular dynamics simulations show significant asymmetry of the "Al on Fe" and "Fe on Al" interfaces for all substrate layer orientations. The "Al on Fe" interface is atomically sharp in case of (001) and (110) oriented Fe layers. Mössbauer spectroscopy measurements of vacuum evaporated Al/Fe/Al and Al/Fe/Ag trilayers support these calculations by showing that the short range properties of the "Al on Fe" interface are similar to that of a Fe layer that is covered with a chemically non-mixing element. We think that the experimental strategy applied can be useful in exploring the chemical mixing at interfaces for different sample deposition conditions and element pairs.

ACKNOWLEDGMENTS

[1]S. Q. Wang and H. Q. Ye, Curr. Opin. Solid State Mater. Sci. **10**, 26 (2006).

[2]J. D. R. Buchanan, T. P. A. Hase, B. K. Tanner, P. J. Chen, L. Gan, C. J. Powell, and W. F. Egelhoff, Jr., Phys. Rev. B **66**, 104427 (2002).

[3]D. C. Meyer, K. Richter, P. Paufler, P. Gawlitza, and T. Holz, J. Appl. Phys. **87**, 7218 (2000).

[4]W. Priyantha, R. J. Smith, H. Chen, M. Kopczyk, M. Lerch, C. Key, P. Nachimuthu, and W. Jiang, J. Appl. Phys. **105**, 053504 (2009).

[5]T. Geilman, J. Chevallier, M. Fanciulli, G. Weyer, V. Nevolin, and A. Zenkevitch, Appl. Surf. Sci. **109/110**, 570 (1997).

[6]M. Carbucicchio, C. Grazzi, M. Rateo, G. Ruggiero, and G. Turilli, Nanostruct. Mater. **11**, 775 (1999).

[7]R. Checchetto, C. Tosello, A. Miotello, and G. Principi, J. Phys.: Condens. Matter **13**, 811 (2001).

[8]D. Kaptás, J. Balogh, T. Kemény, L. F. Kiss, L. Bujdosó, A. Kovács, A. Hirata, and I. Vincze, Phys. Rev. B **75**, 014417 (2007).

[9]S. Jani, V. Sebastian, N. Lakshmi, V. R. Reddy, K. Venugopalan, A. Gupta, and N. P. Lalla, J. Appl. Phys. **104**, 123907 (2008).

[10]J. Noetzel, K. Brand, H. Geisler, A. Gorbunov, A. Tselev, E. Wieser, and W. Möller, Appl. Phys. A **68**, 497 (1999).

[11]C.-Y. Chung and Y.-C. Chung, Mater. Lett. **60**, 1063 (2006).

[12]S.-G. Lee and Y.-C. Chung, J. Appl. Phys. **105**, 034902 (2009).

[13]C. Kim and Y.-C. Chung, Appl. Surf. Sci. **252**, 8380 (2006).

[14]T. Shinjo and W. Keune, J. Magn. Magn. Mater. **200**, 598 (1999).

[15]A. Gupta, D. Kumar, and V. Phatak, Phys. Rev. B **81**, 155402 (2010).

[16]J. Balogh, L. Bujdosó, D. Kaptás, I. Dézsi, and A. Nakanishi, Phys. Rev. B **85**, 195429 (2012).

[17]J. Balogh, L. Bujdosó, D. Kaptás, T. Kemény, I. Vincze, A. Kovács, and L. Tóth, J. Appl. Phys. **105**, 104303 (2009).

[18]D. E. Bürgler, C. M. Schmidt, D. M. Schaller, F. Meisinger, R. Hofer, and H.-J. Güntherodt, Phys. Rev. B **56**, 4149 (1997).

[19]G. Sharma, R. Gupta, D. Kumar, and A. Gupta, J. Phys. D: Appl. Phys. **46**, 505302 (2013).

[20]S. J. Plimpton, J. Comput. Phys. **117**, 1 (1995).

[21]A. Stukowski, Modell. Simul. Mater. Sci. Eng. **18**, 015012 (2010).

[22]X. W. Zhou, R. A. Johnson, and H. N. G. Wadley, Phys. Rev. B **69**, 144113 (2004); X. W. Zhou, H. N. G. Wadley, R. A. Johnson, D. J. Larson, N. Tabat, A. Cerezo, A. K. Petford-Long, G. D. W. Smith, P. H. Clifton, R. L. Martens, and T. F. Kelly, Acta Mater. **49**, 4005 (2001); H. N. G. Wadley, X. Zhou, R. A. Johnson, and M. Neurock, Prog. Mater. Sci. **46**, 329 (2001).

[23]R. A. Johnson, Phys. Rev. B **39**, 12554 (1989).

[24]Q. Ren and H. Gong, Solid. State Commun. **169**, 57 (2013); C. Coline, Intermetallics **11**, 1095 (2003).

[25]R. G. Tissot, Powder Diffr. **18**, 86 (2003).

[26]J. Hesse and A. Rübartsch, J. Phys. E **7**, 526 (1974).

[27]I. Yamada, H. Inokawa, and T. Takagi, J. Appl. Phys. **56**, 2746 (1984).

[28]G. Grüner, I. Vincze, and L. Cser, Solid State Commun. **10**, 347 (1972).

[29]I. Vincze and I. A. Campbell, J. Phys. F: Met. Phys. **3**, 647 (1973).

[30]P. H. Christensen and S. Mørup, J. Magn. Magn. Mater. **35**, 130 (1983).

[31]P. Süle, M. Menyhárd, L. Kótis, J. Labár, and W. F. Egelhoff, Jr., J. Appl. Phys. **101**, 043502 (2007).

[32]P. Süle, L. Kótis, L. Tóth, M. Menyhárd, and W. F. Egelhoff, Jr., Nucl. Instrum. Methods Phys. Res. B **266**, 904 (2008).

[33]P. Süle, Nucl. Instrum. Methods Phys. Res. B **268**, 1404 (2010).

[34]D. R. Askeland, P. P. Fulay, and W. J. Wright, *The Science and Engineering of Materials*, 6th ed. (Cengage Learning Inc., Stamford, 2010).